VX680 Binding in Aurora A: π−π Interactions Involving the Conserved Aromatic Amino Acid of the Flexible Glycine-Rich Loop

ARTICLE *in* THE JOURNAL OF PHYSICAL CHEMISTRY A · FEBRUARY 2011

Impact Factor: 2.69 · DOI: 10.1021/jp108286r · Source: PubMed

3 AUTHORS, INCLUDING:

Taiana Oliveira
European Molecular Biology Laboratory
23 PUBLICATIONS **289** CITATIONS
SEE PROFILE

Richard Alan Engh
University of Tromsoe
109 PUBLICATIONS **6,888** CITATIONS
SEE PROFILE

THE JOURNAL OF PHYSICAL CHEMISTRY A

ARTICLE

pubs.acs.org/JPCA

VX680 Binding in Aurora A: $\pi-\pi$ Interactions Involving the Conserved Aromatic Amino Acid of the Flexible Glycine-Rich Loop

Taianá M. Oliveira, Rafi Ahmad, and Richard A. Engh*

NORSTRUCT, Department of Chemistry, University of Tromsø, 9037 Tromsø, Norway

ABSTRACT: The regulation of protein kinases requires flexibility, especially near the ATP binding site. The cancer drug target Aurora A is inhibited by the ATP site inhibitor VX680, and published crystal structures show two distinct conformations. In one, a refolded glycine-rich loop creates a stacked $\pi-\pi$ interaction between the conserved aromatic residue of the glycine-rich loop hairpin turn (F144) and the inhibitor. This refolding, associated with binding to a peptide derived from the cofactor TPX2, is absent in the other structure. We use surface plasmon resonance to measure VX680 binding to native and mutant F144A Aurora A kinase domains, with and without the TPX2 peptide. Results show that the F144 aromatic side chain contributes 2 kcal/mol to the VX680 binding energy, independent of the TPX2 peptide. This indicates that distinct VX680 bound conformations of Aurora A cannot be simply correlated with TPX2 binding and that Aurora A retains flexibility when inhibitor-bound. Molecular dynamics simulations show that alternate geometries for the $\pi-\pi$ interactions are feasible in the absence of the rigidifying packing interactions seen in the crystal lattice.

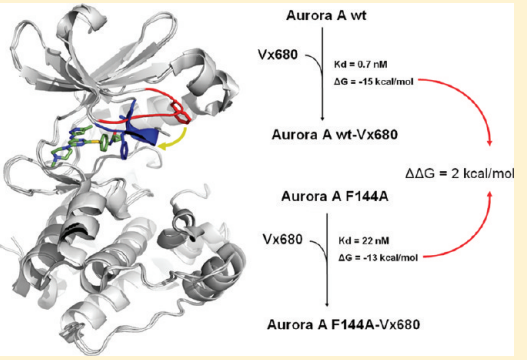

INTRODUCTION

The importance of ligand-induced structural modifications of drug targets has long been recognized,[1−3] and the unpredictability of the changes is one of the major obstacles to in silico methods in drug discovery.[4,5] This is particularly true for protein kinase inhibitors that target the ATP binding pocket.[6,7] Formed by the juxtaposition of the two folding subunits of the catalytic domain, the ATP site exhibits wide-ranging flexibility, including large-scale motions of the individual subunits, local refolding, especially of the activation and glycine-rich loops, and side-chain reorientations. These flexibilities are greater than those for many other enzyme classes because they arise from the mechanisms for strict control of protein kinase activity and substrate recognition, which in turn are required for signaling fidelity.[8,9] The hundreds of crystal structures that are now available for protein kinases[10] show several conformers and point out that some moieties which are highly connected to regulatory control seem to be especially pliable; these include the activation loop, the C-helix, and the glycine-rich loop.

Protein kinases constitute the primary mechanism of cell signaling processes and are thus involved in virtually all aspects of cell function. Consequently, dysregulation of protein kinase activity is a common cause of disease, and protein kinases now constitute the major class of targets for new cancer drugs.[11,12] The Aurora kinases A, B, and C are among the prioritized targets; these serine/threonine protein kinases are pivotal regulators of mammalian cell division. Dysregulated Aurora protein kinase activity can lead to defects in chromatid segregation, genetic instability, and tumorigenesis, and overexpression has been linked to poor prognosis of cancer patients.[13,14]

Of the many Aurora kinase inhibitors now published,[15] VX680 (also called MK-0457) was the first Aurora inhibitor in clinical trials. It is a nanomolar potent pan-Aurora kinase inhibitor, with cross reactivities that notably include inhibition of imatinib resistant Bcr-ABL kinase variants.[16] Although clinical trials with VX680 have been suspended, related inhibitors including VE465 are in active preclinical trials.[17]

Two crystal structures of VX680 in complex with the kinase domain of Aurora A have been reported. In the first, VX680 binds to an inactive conformation of Aurora A, in which the activation loop segment DFGW accommodates the inhibitor via contacts with the two aromatic residues.[18] In the second, VX680 binds to Aurora A, which in turn is complexed to the 43 residue TPX2 activator peptide. This structure differs from the former, especially due to a refolding of the glycine-rich loop, which positions the conserved GxGxFG aromatic residue (Phe144) to make a stacking interaction with the phenyl moiety of VX680.[19]

The conserved glycine-rich loop (consensus motif GxGxxG) is near the N-terminus of the kinase domain and controls ATP binding, activity, and ADP release via solvent exclusion and

Special Issue: Graham R. Fleming Festschrift

Received: August 31, 2010
Revised: January 4, 2011

dx.doi.org/10.1021/jp108286r | J. Phys. Chem. A XXXX, XXX, 000–000

fixation of the nontransferable α and β phosphates. The γ phosphate is left solvent-exposed and poised for transfer to the substrate. The conservation of the glycines may be attributed to both the spatial requirements for phosphate binding[20] and functional flexibility of the loop.[21,22] The residues between the final two conserved glycine residues form a beta hairpin turn, and the latter of these is nearly absolutely conserved as an aromatic residue, usually phenylalanine. One function proposed to explain its conservation is to shield the transphosphorylation reaction from bulk solvent.[23] A second possibility for the conservation as an aromatic side chain may be a role in the stabilization of inactive conformations of the kinases. Several of the crystal structures show hydrophobic and aromatic−aromatic interactions to residues in the activation loop (e.g., the phenyalanine in the DFG motif and the residue succeeding the DFG motif).

The aromatic side chain of the glycine-rich loop hairpin turn is also often involved in binding to inhibitors. Examples of kinase−inhibitor complexes showing such contacts include Aurora A−VX680, 3E5A,[19] Rho kinase−fasudil, 2F2U,[24] FGF receptor−SU5402,[25] 1FGI, PKA−staurosporine, 1STC,[26] and Abl−imatinib, 2HYY.[27] These structures reveal how the glycine flap may refold inward toward the ATP cleft, making favorable contacts with the inhibitor. Resistance mutations[28] at this position have been reported to arise in protein kinases, including Abl[27] and PDGFRα.[29]

To examine the role of the aromatic residue in VX680 binding of Aurora A and interpret the published crystal structures, we introduced the mutation F144A into the glycine-rich loop and measured VX680 binding. Our results show a loss of binding strength when the aromatic side chain is truncated by about 2 kcal/mol. This is in general agreement with the energy loss illustrated by molecular dynamics (MD) simulations that compare native and mutant model systems. We also use steered molecular dynamics to explore alternate conformations that may allow contacts between F144 and the inhibitor. Taken together, our results support a model in which the aromatic−aromatic interaction is a key binding determinant of VX680 binding in uncomplexed Aurora A, most likely with multiple conformations. This affects strategies for drug design of other inhibitors that can utilize analogous aromatic−aromatic interactions.

EXPERIMENTAL METHODS

Protein Production. Recombinant native and mutated kinase domains of Aurora kinase A (residues 120−395) were solubly expressed in *Escherichia coli* BL21(DE3)RIL cells (Stratagene). Site-directed mutagenesis in the Aurora-coding sequence was done via the QuikChange kit (Stratagene) according to the manufacturer's instructions and verified by DNA sequencing. Both Aurora forms were purified to near homogeneity by affinity chromatography trap SP FF (GE Healthcare). Phosphorylation states were monitored by MS−MS spectrometry. TPX2 was custom-synthesized by GLS Biochem Shanghai Ltd.

Binding Studies. Enzymatic activity was determined using the coupled spectrophotometric method from Cook.[30] Varying amounts of ATP were incubated with both forms of Aurora A with and without VX680 at 25 °C in a buffer containing 100 mM MOPS (pH 7.0), 10 mM $MgCl_2$, 100 mM KCl, 1 mM phophoenolpyruvate, 0.1 mM Kemptide, 15 U of pyruvate kinase, 10.5 U of lactic dehydrogenase, and 152 mg/mL of NADH. VX680 dissolved in DMSO was added to give a final concentration of 10 nM.

Biacore CM5 amine coupling sensor chips were activated according to manufacturer's protocols. Immobilization of both Aurora constructs was performed at 25 °C at a flow rate of 30 μL/min using HBS-EP as the running buffer. The proteins (1.75 mg/mL in 100 mM BIS TRIS, pH 6.8) were then covalently coupled to the sensor chip, and excess reactive groups were deactivated with 70 μL of 1 M ethanolamine adjusted to pH 8.5. Control experiments were performed using blank sensor chips. The amount of immobilized native and F144A Aurora were determined to be 7959.7 RU and 8171.5, respectively.

A 1 mM VX680 stock solution in 100% DMSO was used to prepare 100, 50, 20, 10, 5, and 2 nM solutions of VX680 in 50 mM PBS with 250 mM of NaCl and 5% DMSO. 100 μM ATP and 100 μM glucose solutions served as positive and negative controls, respectively, to test binding onto the Aurora immobilized chips. The run was started with three cycles of injection of the running buffer, followed by sample injection cycles. The analysis cycles consisted of a 60 s sample injection (40 μL/min), 200 s of buffer flow (dissociation phase), followed by a regeneration with running buffer, this time injected with a 100 μL/min flow rate, and finally a 30 s carryover cycle. The flow cell temperature was 25 °C. Between sample series, a solvent correction cycle was run according to the instrument manual to adjust for referencing errors due to refractive index differences between running buffer and samples. For Aurora−TPX2 and Aurora−VX680−TPX2 binding measurements, TPX2 was dissolved in HBS-EP buffer (GE Healthcare) to give concentrations of 800, 400, 200, 100, 50, 10, 5, 2.5, and 1.25 nM. Controls were the same as those previously cited. The Aurora−TPX2 run was started with three cycles of injection of the running buffer, followed by sample injection cycles. The analysis cycles consisted of a 150 s sample injection varying from 90 to 150 s (40 μL/min), 600 s of buffer flow (dissociation phase), followed by a regeneration with running buffer injected with a 100 μL/min flow rate, and finally a 30 s carryover cycle. The flow cell temperature was 25 °C. To avoid the use of DMSO solutions and the necessary solvent correction cycles, we chose to measure the binding of TPX2 to the Aurora−VX680 complex. The Aurora−VX680−TPX2 run was started with a capture step in which a 1 mM VX680 solution with 5% DMSO was injected, succeeded by a washing 800s step with the running buffer, HBS-EP saturated with VX680. This was followed by three cycles of injection of the running buffer, followed by sample injection cycles. The analysis cycles consisted of a 150 s sample injection (40 μL/min), 600 s of buffer flow (dissociation phase), followed by a regeneration with running buffer injected with a 100 μL/min flow rate, and finally a 30 s carryover cycle. The flow cell temperature was 25 °C.

A Biacore T100 analytical system was used to record the resonance signal throughout each experiment. Analyses were performed with Biacore T100 Evaluation software version 2.0.1. K_d values were obtained by the steady-state affinity analysis option from the software. In the cases where TPX2 was used as the ligand, kinetics analysis and k_{on}/k_{off} rate estimations were possible for the sensograms from lowest concentrations (nanomolar range).

Molecular Dynamics Simulations. The following structural models were used as the starting structures to perform MD simulations: (1) 3E5A, the crystal structure of Aurora A in complex with VX-680 and TPX2 (PDB ID: 3E5A[19]), (2) 3E5A_F144A, same as 1 but with atoms of F144 truncated to CB (alanine); and (3) 1OL5_VX680, the X-ray structure of Aurora A and bound TPX2 (PDB ID: 1OL5[31]), with VX680 manually docked to the ATP site. All other ligands, for example, ADP, magnesium, and sulfate ions, were deleted from the

structures. Nonhydrogen atoms not modeled in the crystal structures were added using the AMBER10 software package.[32] Hydrogen atoms were added to the structures using the protein preparation wizard of the Schrodinger suite (Schodinger Inc., Portland, OR). Amber force field parameters for phosphorylated threonine residues were taken from Homeyer et al., 2006.[33] Parameters for VX680 were derived from semiquantum chemistry calculation AM1-Bcc invoked in the antechamber module of the AMBER package. Crystallographic waters were kept, and in addition, water molecules were added using the TIP3P model around the molecular models with a 10 Å buffer from the edge of the periodic box. Counter ions were added to achieve total charge neutrality.

The AMBER10 biomolecular simulation package was used for all of the MD simulations. Force fields applied for proteins and the organic ligand were amber99SB and gaff, respectively. The molecular mechanics Poisson−Boltzmann surface area (MM-PBSA) and molecular mechanics generalized Born surface area methods (MM-GBSA) were used to calculate the binding energy and the per-residue free-energy decomposition of the protein−ligand complex, respectively. Prior to MD simulations, the molecular systems were subjected to 5000 steps of steepest energy minimization of the water with the protein/protein−ligand complex fixed and then 5000 cycles of minimization of the whole system. The first 2500 minimization steps used steepest descent, whereas the last 2500 steps used the conjugate gradient method. The temperature of the system was raised stepwise (for 50 ps) to the final temperature of 298 K and kept constant for the rest of the simulation. This was followed by an equilibration period of 200 ps. The production phase of the simulations was carried out for 20 ns in the isothermal−isobaric ensemble using 298 K as the temperature and 1 atm of pressure. A 10 Å cutoff for nonbonded interactions was used in the simulation, and the Particle Mesh Ewald method was used to handle long-range interactions. SHAKE was applied to restrain covalent bonds involving all hydrogen atoms. Coordinates were written to file every 0.5 ps during the production phase.

Steered Molecular Dynamics (SMD). SMD applies an external force onto a physical system and drives a change in coordinates with a certain time. This methodology can be used to drive physical process such as conformational changes from the binding/unbinding of ligands. In this study, SMD simulations were used to explore alternate reconfigurations of the G loop, in the presence of VX680, that enable aromatic−aromatic interactions with F144. Three conformations of 1OL5_VX680 (i.e., 0.25, 10, and 20 ns from the MD production period) were used as initial structures for SMD. SMD was performed over 100 000 steps with a time step of 0.002 ps. The driving force constant, 50 kcal/(Å2 mol), was applied to the centroids of the two rings. The aromatic ring of Phe144 was driven from its original position (14 Å away) to 4 Å away from the corresponding aromatic ring of VX-680, forming an aromatic−aromatic interaction. Each simulation was repeated two times.

RESULTS

Binding of VX680. We performed the SPR binding studies to investigate the interactions between Phe144 and VX680 in Aurora A in solution, in particular, to see if the glycine-rich loop refolding occurs in solution and whether TPX2 plays a role. The SPR binding analysis for VX680 and the wild-type Aurora A kinase domain construct reveals a K_d of 0.7 nM, in good agreement with a previously reported K_d value of 0.6 nM.[34]

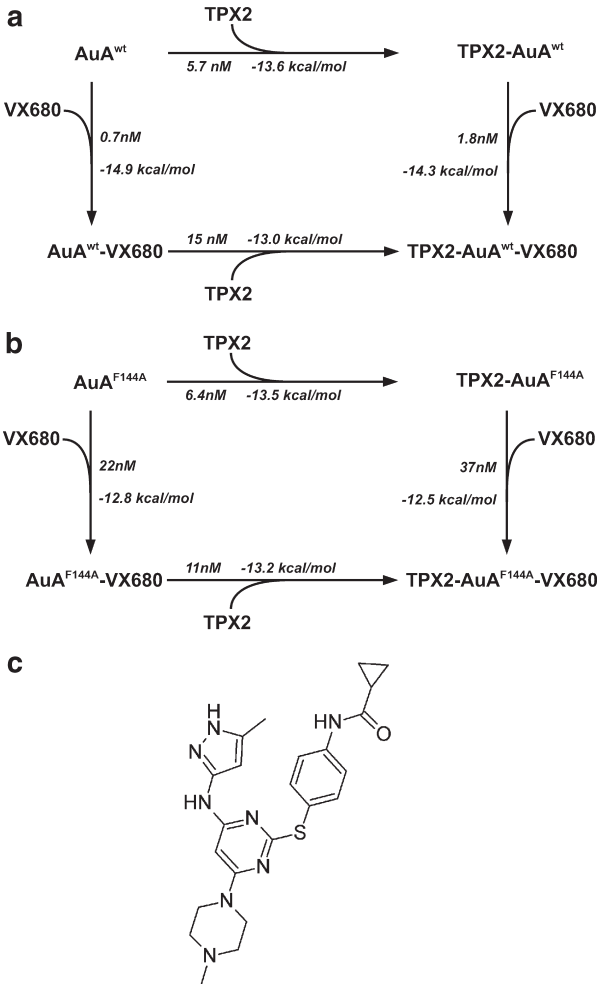

Figure 1. Thermodynamic cycle depicting the formation of the ternary complex VX680−Aurora−TpX2 for (a) wild-type and (b) F144A mutated Aurora A. K_d and ΔG values for TPX2 binding and for VX680 binding to the Aurora monomer are derived from surface plasmon resonance measurements; the values for VX680 binding to the Aurora−TPX2 dimer are calculated from the thermodynamic cycle. (c) Chemical structure of the ATP antagonist pan Aurora inhibitor VX680 used in this study.

The SPR binding assay for the F144A Aurora A mutant showed a K_d of 21.6 nM, weaker than that for wild-type by about 30 fold (Figure 1). In both cases, it was not possible to obtain k_{on}/k_{off} rates as they were too fast for quantitative evaluation. Therefore, the K_d values reported here were calculated from equilibrium responses of VX680 injections at various concentrations. The sensograms for the interaction of F144A mutant and VX680 are presented in the box within Figure 1. Free-energy values for the binding were calculated by the formula $\Delta\Delta G = -RT\ln(K_{d1}/K_{d2}) = 2$ kcal/mol, that is, truncation of the phenyl group from F144 weakens binding of VX680 by 2 kcal/mol.

Effect of TPX2 on VX680 Binding. To test whether the presence of TPX2 affects VX680 binding, for example, by promoting the refolding of the glycine flap and the interaction with F144, we also assessed its K_d for the Aurora−TPX2 complex with both native and F144A. As described above, the assessment was made indirectly by measuring of the K_d of TPX2 to the Aurora constructs, both unbound and bound by VX680, and relating the dissociation constants through the thermodynamic

dx.doi.org/10.1021/jp108286r |J. Phys. Chem. A XXXX, XXX, 000–000

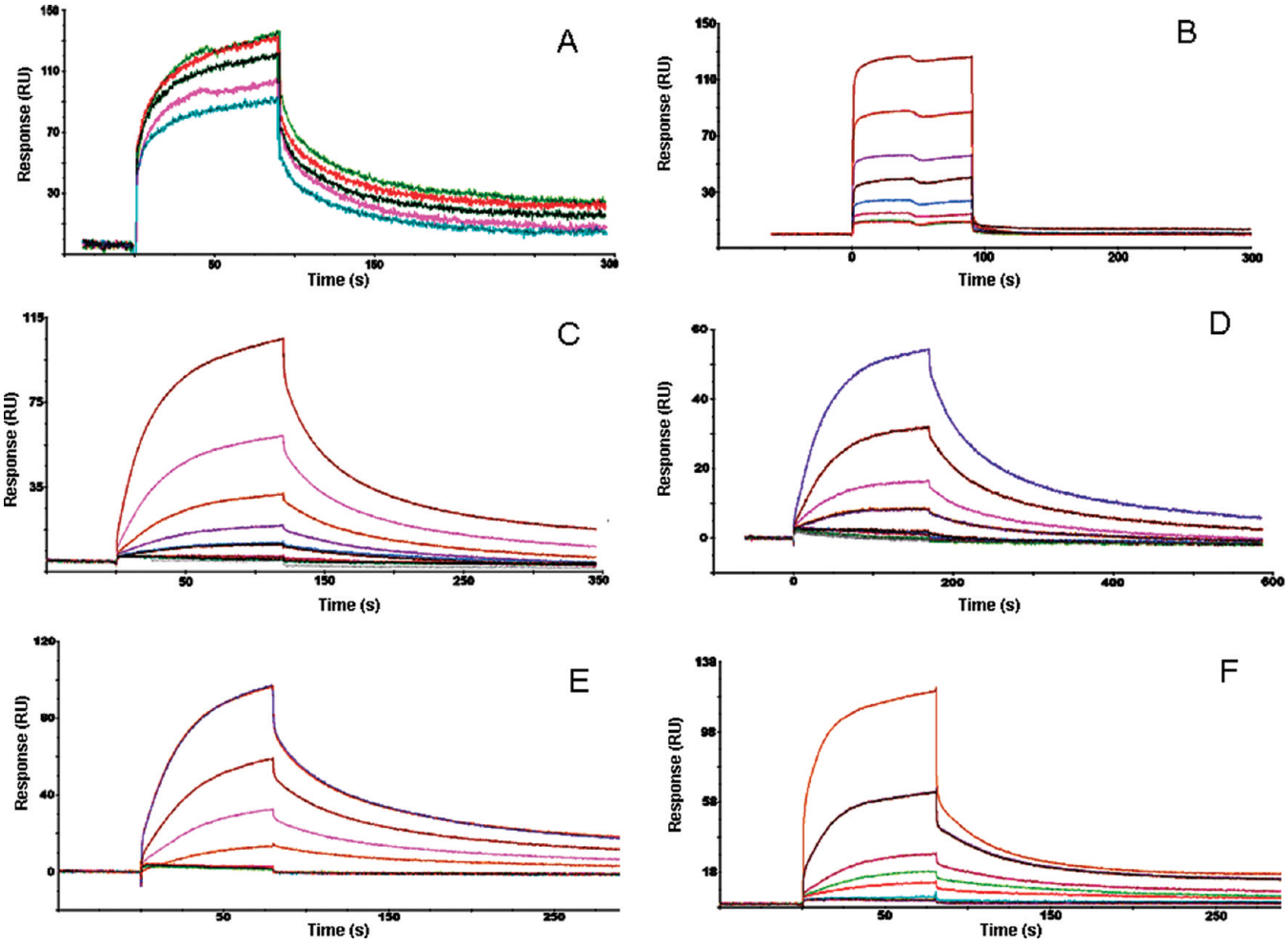

Figure 2. Surface plasmon resonance sensograms portraying the binding of (a) VX680 to Aurora A wild-type, (b) VX680 to Aurora A F144A, (c) TPX2 to Aurora A wild-type, (d) TPX2 to Aurora A F144A, (e) TPX2 to Aurora A wild-type−VX680 complex, and (f) TPX2 to Aurora A F144A.

cycle of the formation of the ternary complex Aurora−TPX2−VX680 (Figure 1). The cycle shows the two possible paths of sequential binding for formation of the ternary complex, which implies the relationship $K1 \times K3 = K2 \times K4$, whereby the K's represent the association constants for ($K1$) binding of TPX2 to Aurora A, ($K3$) binding of VX680 to the Aurora−TPX2 complex, ($K2$) binding of VX680 to Aurora A, and ($K4$) binding of TPX2 to the Aurora A−VX680 complex. Thus, the K_d of VX680 to Aurora−TPX2 may be calculated from the other three rates. SPR binding analysis of TPX2 to uncomplexed Aurora revealed K_d values of 5.7 and 6.4 nM for the native and mutant constructs, respectively. The corresponding values of binding of TPX2 to Aurora−VX680 complexes were 15 and 11 nM. Thus, the thermodynamic cycle reveals a K_d of 1.8 nM for VX680 binding to the Aurora wild-type−TPX2 complex and 37 nM for VX680 binding to the Aurora F144A−TPX2 complex. Given those values, the loss of binding energy due to the mutation in the presence of TPX2 is 1.8 kcal/mol, very similar to the energy difference in the absence of TPX2. All sensograms are shown in Figure 2.

TPX2 Binding Rates. The k_{on} and k_{off} rates were determined for TPX2 binding by a kinetic evaluation of the sensograms fitting a 1:1 Langmuir binding model. Instrument limitations resulted in detection limits of 10^4 to 5×10^6 $M^{-1}s^{-1}$ for the association constant k_{on} and of 10^{-1} to 10^{-5} s^{-1} for the dissociation constant k_{off}. Given that k_{on} values were outside of these detection limits, k_{on} values were deduced from the $K_d = k_{off}/k_{on}$ equation. Notably, the k_{on} and k_{off} rates are doubled for the mutant F144A (12×10^3 M^{-1} s^{-1} and 7×10^{-5} s^{-1}, respectively) as compared to the wild-type (5×10^3 M^{-1} s^{-1} and 3.4×10^{-5} s^{-1}), which is consistent with the deletion of the bulky aromatic moiety. Thus, both binding and release of TPX2 seem to involve displacement of the aromatic residue for TPX2 binding. This holds true for the binding of TPX2 to the Aurora−VX680 complex as well; the mutant F144A has slower k_{on} and k_{off} rates (4.5×10^3 M^{-1} s^{-1} and 5×10^{-5} s^{-1}, respectively) compared to the wild-type (8×10^3 M^{-1} s^{-1} and 12×10^{-5} s^{-1}). Crystal structures show contacts of TPX2 with helix C and also between helix C and the glycine-rich loop; therefore, such effects may be mediated by helix C. For both the wild-type and the mutant, the presence of VX680 slows the k_{on} rate and accelerates the k_{off} rate for TPX2 binding.

Kinase Activity. To exclude artifacts of the F144A mutation on, for example, ATP site geometry or activity, K_m values for ATP of Aurora A wild-type and F144 Aurora A were determined using the Cook assay (see Experimental Methods). As Aurora A wild-type shows a $K_{m,ATP}$ of 38 ± 6 μM, and Aurora A F144A shows a $K_{m,ATP}$ of 42 ± 6 μM; the mutation does not influence the ATP binding or the kinase activity of the protein in vitro. As a second control, LC-Q-ToF analysis of the Aurora peptides derived from

dx.doi.org/10.1021/jp108286r |J. Phys. Chem. A XXXX, XXX, 000–000

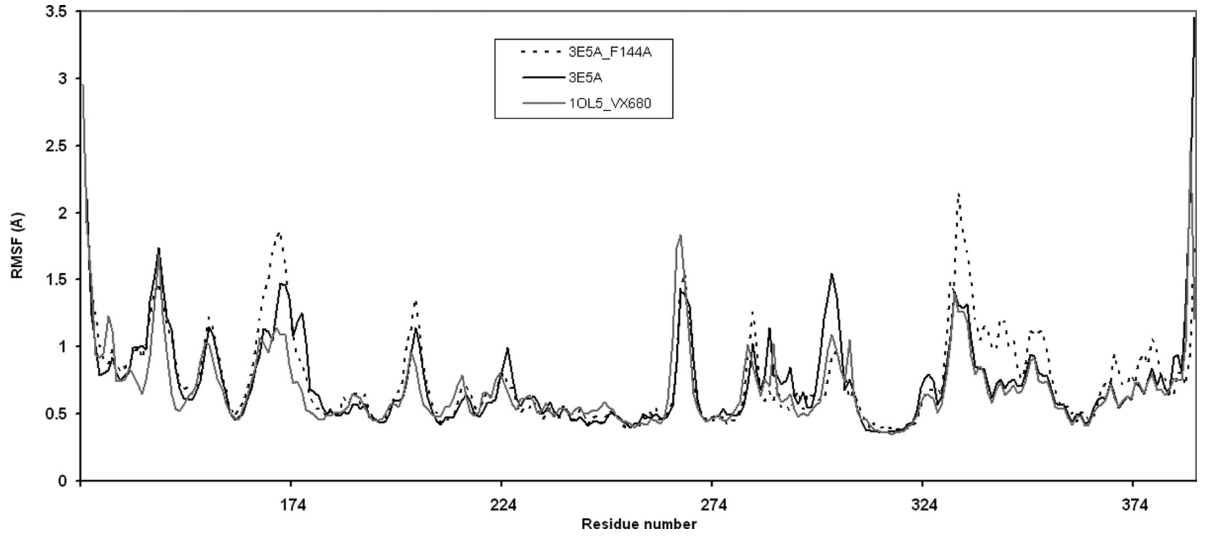

Figure 3. Root-mean-square atomic fluctuations (RMSF) observed in the MD simulations of the three different systems, 3E5A-based Aurora A F144A complexed with VX680 (dotted line), 3E5A-based native Aurora A complexed with VX680 (black continuous line), and 1OL5-based Aurora A complexed with VX680 (gray continuous line). The RMSF per residue was calculated based on the amino acid backbone atoms in the minimized average structure from the production phase and the sampled trajectory from the simulation. The amino acid numbering of PDB entry 3E5A has been used here.

tryptic digestion revealed that both the Aurora A wild-type and Aurora A F144A proteins used for the binding studies were not phosphorylated.

MD Simulations. The simplest interpretation of the SPR results is that the phenyl group of F144 makes a direct interaction with VX680. Further, it is simplest to assume that this interaction is of the form seen in PDB structure 3E5A, in the absence of further structural information. To explore this scenario and compare MD predictions of aromatic−aromatic interaction geometries with experiment, MD simulations were conducted of the binding of VX680 to three different forms of Aurora A, (1) with the refolded glycine-rich loop, (2) with the refolded glycine-rich loop coupled with the mutation F144A (truncation of side-chain atoms), and (3) with extended glycine-rich loop, PDB structure 1OL5. In all three models, the fold of the enzyme was stable over the 20 ns MD simulations. The regions of greatest fluctuation were the N- and C-termini, together with the glycine-rich loop, helix B, and the loop between helix C and beta strand-4, beta strand-8, and α helix-8, as depicted in Figure 3.

The average structures from the 20 ns simulations are close to the crystallographic structures from which they are derived, with VX680 shifted by about 0.1 Å rmsd. In all three simulations, VX680's piperazine moiety is rather flexible. The free-energy calculations show that residues L139, Y212, A213, L215, T217, and L263 that are in the solvent exposed and in the front hydrophobic pocket of the kinase ATP cleft contribute most to the binding energy. In addition, residues V147, A160, L194, L210, and E211 of the selectivity or hydrophobic back pocket also contribute significantly. The residue-based energy decompositions of the interaction energy between the three Aurora A−VX680 complexes are shown in Figure 4.

Over the course of the simulation of VX680—Aurora in the refolded glycine-rich loop conformation, the glycine-rich loop generally retains its conformation (Figure 5, left). However, Phe144 assumes several different rotamer conformations, with accompanying variation in the interaction with the inhibitor (Figure 5, right), all the while staying within contact distances typical for $\pi-\pi$ interactions.[35] While the initial conformation shows a face-to-face geometry for the interaction of Phe144 with the phenyl group of VX680, the MD trajectory shows, in addition, several edge-displaced and parallel-displaced configurations. This deviation from the crystal structure is not evidence of a deficiency of the force field as the model system does not have crystal contacts (see Discussion). In general, the stability of the structures over the course of the simulations is consistent with the anchoring interactions (Figure 6a), and the time scale of the structural transition will be considerably longer than the 20 ns of the simulations.

The total free-energy difference estimated by the MD runs includes effects that are indirectly or spuriously connected to the mutation. Figure 3a and b shows the decomposition of the energy per residue and per energy type for F144. These show that the energy difference for the mutation can be considered to arise primarily from the loss of van der Waals interactions between F144 and the inhibitor. The simulation estimates this energy at approximately 1 kcal/mol and is a reasonable estimate, particularly considering that the aromatic−aromatic interaction energies for small aromatic moieties are predominantly van der Waals in character.[36] A more precise estimate for the aromatic−aromatic interaction energies would require knowledge of the full range and populations of conformations taken by the aromatic moieties, and greater accuracy would require parametrizations beyond current capacities. The total binding energy difference will involve other effects, including structural adjustments resulting from the loss of the aromatic side chain. The MD simulations show examples of these.

Steered MD Simulations. These simulations were performed using native Aurora to explore possible glycine-rich loop refolding pathways upon binding to VX680 (Figure 6). The force of the steered MD drew the aromatic moieties of VX680 and F144 together as intended. However, the resultant refolding was different from the crystal structure. Again, this is not evidence of a deficiency of the force field of the simulation (see discussion of crystal contacts below). Instead, it is a demonstration of the plausibility of generating aromatic−aromatic interactions without the need to traverse energy barriers, as seen in the crystal structure transition (Figure 6c and d). During the course of the

dx.doi.org/10.1021/jp108286r |J. Phys. Chem. A XXXX, XXX, 000–000

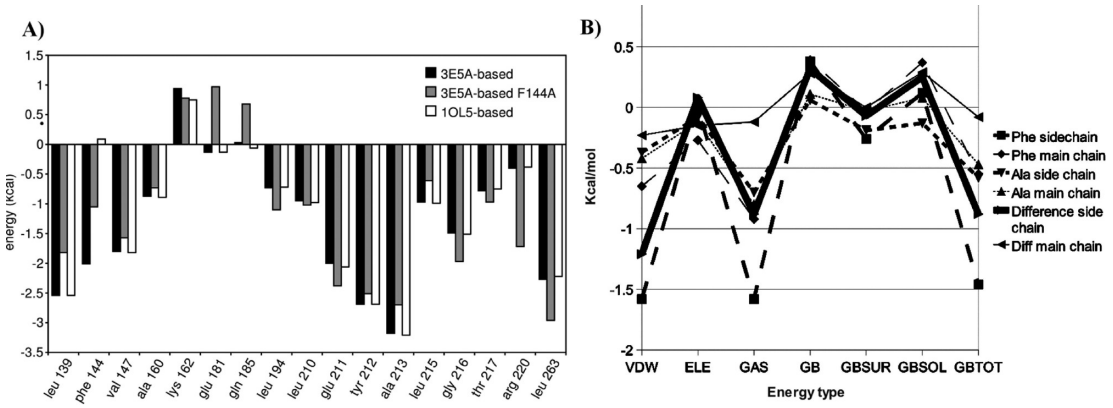

Figure 4. Aurora−VX680 interaction energy decompositions showing contributions of key residues for the MD runs. The total interaction energy difference generated by the substitution F144A is roughly twice that of the aromat−aromat interactions alone. (a) Comparisons of specific residues show that the total loss of binding interaction energy from the F144A substitution alone (∼1 kcal/mol) is roughly the same order of magnitude as other effects, including structural changes involving polar residues Glu181, Gln185, and Arg220, as well as other nonpolar effects. (b) Decomposition of the interaction energies involving F144 and its mutant analogue A144 show the energy difference to be dominated by the van der Waals energy term (VDW) for the side chain and not electrostatics (ELE), reaction field energy (GB), or hydrophobic solvation free energy (GBSUR), as expected. The remaining terms involve sums of these: GAS (total gas phase energy) = VDW + ELE, GBSOL (sum of nonpolar and polar contributions to solvation) = GB + GBSUR, GBTOT (final estimated binding free energy) = GBSOL + GAS.

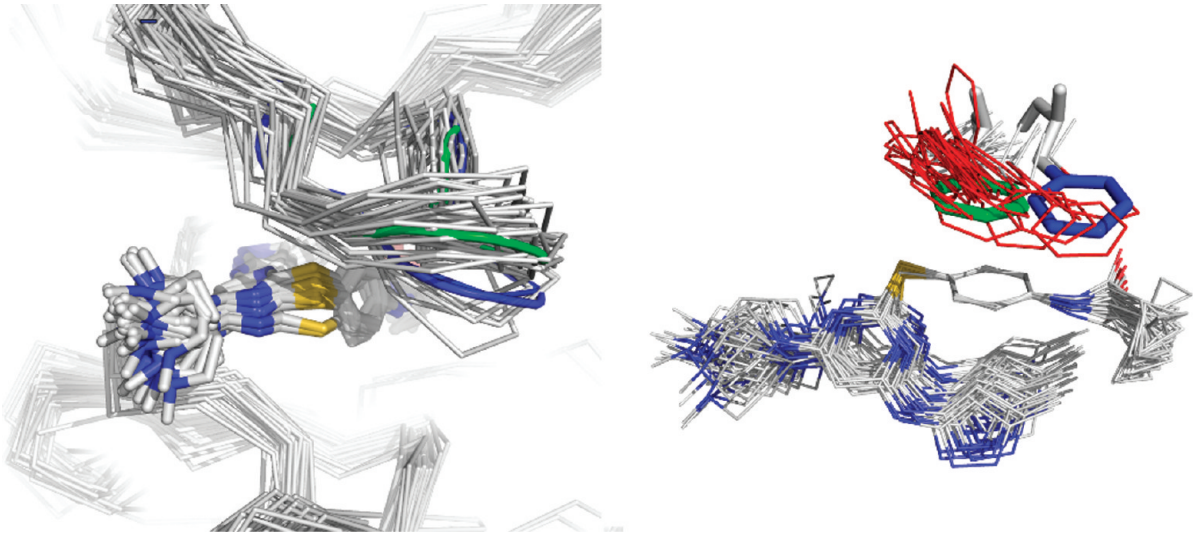

Figure 5. Superpositions of 40 configurations sampled from the MD runs at 0.5 ns intervals. (left) The glycine-rich loop backbone and VX680 of the 3E5A-based Aurora−VX680 system, aligned using the VX680 atomic coordinates. The initial conformation of the loop is highlighted green, and the final conformation is blue. (right) The distribution of Phe144−VX680 $\pi-\pi$ geometries of the MD run of the 3E5A-based Aurora−VX680 system. The structures were aligned using the VX680 aromatic moiety in contact with F144. The initial conformation of F144 is highlighted green, while the final conformation is blue.

steered MD, the trajectories of the Ramachandran dihedral angles remained within the energetically favorable regions, as seen at the outset of the simulation.

DISCUSSION

The published structural studies of VX680 binding identify the refolding of the glycine-rich loop as a critical selectivity determinant, associated with the binding of the cofactor TPX2.[18] Both the refolding and cofactor binding phenomena highlight difficulties of analyzing protein kinase selectivity patterns with bioinformatics and even experimental profiling techniques; refolding effects are generally not predictable, and cofactors cannot be included in any comprehensive fashion. Both Abl and Aurora A have shown glycine-rich loop refolding phenomena connected to VX680 binding but share relatively low sequence similarity even in the glycine-rich loop region. For Aurora, the refolding has been seen in a published crystal structure only in connection with TPX2 peptide binding. However, it is not clear if TPX2 may cause or contribute to the refolding. We demonstrate here that the glycine-rich loop aromatic residue F144 plays a key role in VX680 tight binding also in the absence of TPX2 peptide binding, and we argue that this is from direct $\pi-\pi$ interactions between F144 and the inhibitor.

The extended glycine-rich loop structure of most Aurora A structures shows Phe144 to be anchored to residues L164, L169, A172, and V174 via hydrophobic and C−H/π interactions and also to K143 via a cation−π interaction[19,31,37−47] (Figure 6a and b).

dx.doi.org/10.1021/jp108286r |J. Phys. Chem. A XXXX, XXX, 000–000

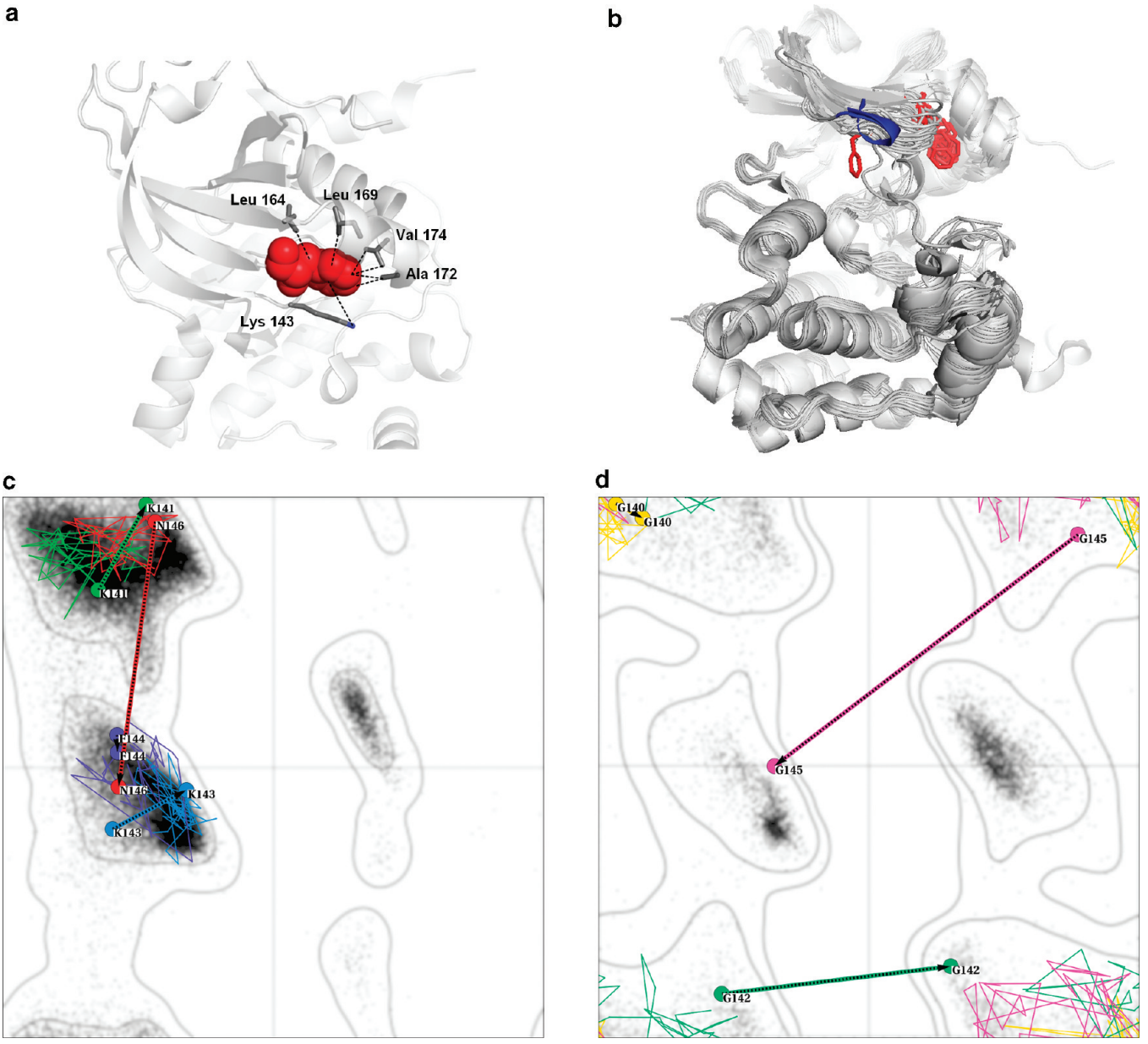

Figure 6. Aurora A glycine-rich loop conformations of published crystal structures. (a) Anchoring interactions involving Phe144 (red) in most of the Aurora crystal structures. In 85% of the human Aurora A structures, Phe144 interacts with L164, L169, A172, and V174. K143 is seen to provide an anchor via salt bridge interactions with varying partners from, for example, helix C and the activation loop (PDB codes: 3J4Z, 2W1C, 2W1D, 2W1E, 2W1F, 2W1G, 3COH, 3FDN, 3HOY, 3HOZ, 3H10, 3HOZ, 3HAG, 1MQ4, 1MUO, 1OL5, 1OL6, 1OL7, 2BMC, 2DWB, 2J50, 3DAJ, 3E5A, 3EFW). (b) Superposition of the folds of the available human Aurora A X-ray structures. The glycine-rich loop conformations are generally extended, but in 3E5A, it adopts a refolded conformation (blue). Phe144 is shown in red. (c) Ramachandran plot of the nonglycine residues of the glycine-rich loop, with energy contours from Lovell et al.[56] The transitions seen between the extended (1OL7) and refolded (3E5A) structures are shown as arrows. The steered MD trajectories are shown with the same color codes. (d) Same as (c) but showing instead the glycine residues of the glycine-rich loop and glycine Ramachandran energy contours.

Table 1. Summary of VX680−Protein Complex Crystal Structures

PDB	content	description
n/a	AuA + VX680	DFG out activation loop is not phosphorylated and otherwise disordered; glycine-rich loop is extended
3E5A	AuA + VX680 + TPX2 (1−42)	DFG in activation loop is a phosphorylated, refolded glycine-rich loop with face−face F144−inhibitor interactions; crystal contacts to glycine-rich loop
2F4J, 3NSV	ABL (T315I) + VX680, ABL2 + VX680	DFG in is an unphosphorylated, refolded glycine-rich loop with glycine-rich loop aromatic residue (Tyr)−inhibitor interactions; no crystal contacts to the loop

dx.doi.org/10.1021/jp108286r |J. Phys. Chem. A XXXX, XXX, 000–000

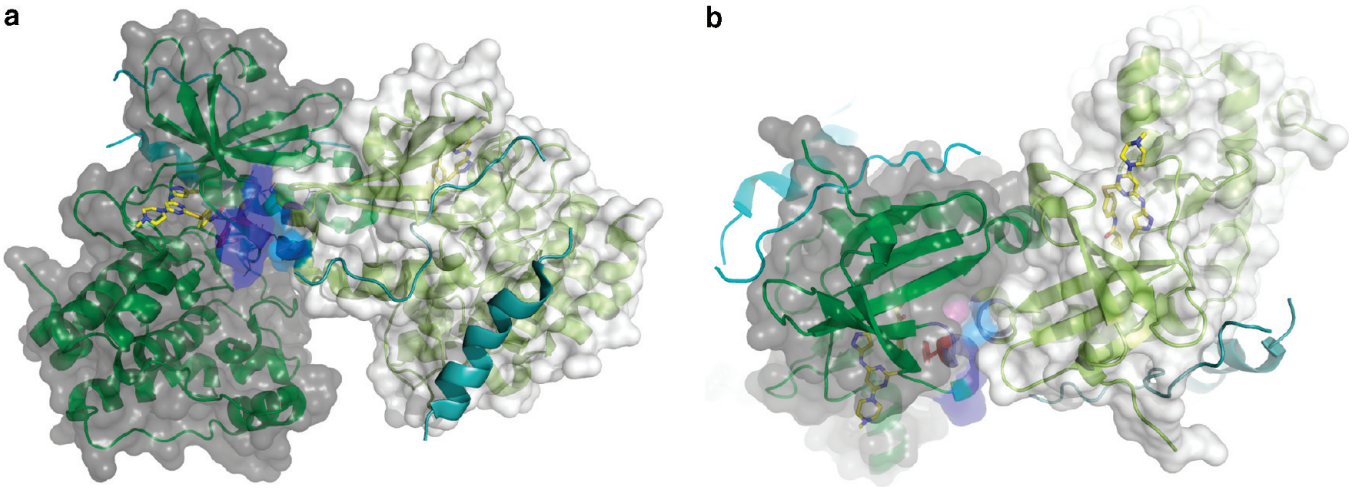

Figure 7. Orthogonal views of the crystal packing/dimerization interface of 3E5A. The TPX2 peptide is shown in cyan, the refolded glycine-rich loop in blue, and F144 in red/magenta. The buried surface area of the dimer interface, including the surface involving the glycine-rich loop, is much more extensive than inhibitor interactions.

The published VX680 crystal structures are summarized in Table 1. One[18] binds to Aurora in an inactive "DFG out" conformation, as discussed above. The other two bind to Aurora A[19] and the drug resistant Abl mutant T315I.[48] Both of these are in the "DFG in" conformation with differing glycine-rich loop refolding transitions that enable aromatic−aromatic interactions between the loop and the inhibitor.

Our binding results show that unphosphorylated TPX2 peptide-free Aurora A loses a significant part of its affinity for VX680 when Phe144 is mutated to alanine. This in turn suggests that the glycine-rich loop also can be refolded in the unphosphorylated Aurora A kinase domain. In addition, this loss of affinity continues to exist in the presence of TPX2, given that the difference in free energy is just slightly decreased in the case of TPX2-bound Aurora (by 0.4 kcal/mol).

Aromatic−aromatic interactions have long been recognized as important to protein structure and ligand binding.[49,50] Statistical analysis from the protein data bank of the preferential geometries of interacting pairs of aromatic residues revealed that parallel-displaced geometries are most common.[51] VX680 in TPX2 (1−43)/Aurora (3E5A) is seen with a minimally displaced face−face interaction with the glycine-rich loop F144, and in ABL(T315I), it is with significant displacement and rotation (2F4J) with Y253. The observation of two types of interactions with two crystal structures hints at the existence of more. Studies of the energetics of aromatic−aromatic interactions[36] show that energies between different geometries do not differ greatly, and for example, competition between face−face and edge−face geometries is strongly affected by the polarity of the environment and the ability of the surrounding solvent to form hydrogen bonds.[51] The lack of clear energy minima for the interaction geometry is further evidence of the likelihood of a range of geometries involved in the interaction. The MD simulations showed a range of geometries for the aromatic−aromatic interactions (Figure 5, right). These are plausible alternatives for the interactions as they might occur in the absence of rigidifying crystal contacts.

The glycine-rich loop of structure 3E5A is strongly involved in crystal contacts (Figure 7). Analysis server CryCo 5.2[52] shows that each residue from the glycine-rich loop has at least one crystal contact within 5 Å, while POPS[53] calculates a buried surface area of 387.30 Å^2 for the interface with the glycine-rich loop alone. The entire crystal packing interface is much larger and seems likely to have played a significant role in fixing the glycine-rich loop into a conformation most compatible with crystallization. This supports the view that VX680 binding in the absence of crystal contacts will involve multiple conformations, including aromatic−aromatic interactions with geometries different from those seen in 3E5A.

The Aurora A−VX680 binding as measured by SPR, giving a $\Delta\Delta G_{EXP}$ of 2 kcal/mol, is in good agreement with estimates of the $\pi-\pi$ interaction energies of Phe-Phe interactions in proteins (1−3 kcal/mol[35]), with the differential free energies of binding as estimated by the MD runs ($\Delta\Delta G_{MD}$ = 2.7 kcal/mol) but also with a simple estimate based on a simple buried surface area estimate. With an area of 39 Å^2 buried in the face−face interaction of 3E5A F144, an interaction energy of about 1 kcal/mol is predicted from a model of 30 cal/mol/Å.[28]

The TPX2 peptide (1−43) has been used to study modulation of Aurora by the TPX2 protein; Bayliss and coauthors reported that the activating effect of TPX2 is fully retained in this peptide.[31] Kinetic studies by Anderson and co-workers[54] show that the stimulating effect of TPX2 arises from increased affinity to both ATP and peptidic substrates and not by increasing the intrinsic catalytic activity (k_{cat}). Here, we demonstrate that the binding of TPX2 to the native protein and our F144A mutant is practically unchanged (5.7 and 6.4 nM, respectively), although the rates of binding are shifted. Analyzing the TPX2−Aurora interaction from the crystal structure in the 1OL5 PDB file, we find a buried surface area of 2570 Å^2, corresponding roughly to a free energy of association of −13 kcal/mol. A K_d estimated from this would be some 30 nM, a factor of 5 weaker than the measured value but still in the nanomolar range. The solvation free-energy gain is estimated to be −16 kcal/mol; thus, the formation of a hydrophobic interface between the protein and the peptide dominates. TPX2 is a possible target protein for pancreatic cancer therapies. Given the difficulties of achieving therapeutic selectivity for many protein kinase inhibitors and also given the fact that TPX2 has been shown to decrease binding of inhibitors occupying the so-called hydrophobic selectivity pocket, the possibility of targeting the Aurora−TPX2 interaction looks especially attractive. However, our binding data reinforce the view that targeting such a strong protein−protein interaction is, at best, challenging.

dx.doi.org/10.1021/jp108286r |J. Phys. Chem. A XXXX, XXX, 000–000

Our analysis should shed some light onto selectivity determinants for other compounds similar to VX680. Bebbington and collaborators connect the cross reactivity of VX680 with Flt-3 and Abl to its ability to bind to pockets that are unavailable in the active conformation of the kinase.[55] If a state with an inactive T-loop fold and a refolded glycine-rich loop simultaneously exist in significant proportions (as suggested by our results), this must be taken into account. The Abl—VX680 structure has already revealed that binding is not incompatible with an active conformation of the T-loop, and further, it reveals a similar bent configuration for the glycine-flap. This binding mode seems to be more compatible with FLT3 as it has a phenylalanine in the gatekeeper position, which together with a inactive conformation of the T-loop would limit the access of the inhibitor to the pocket formed by the inactive conformation.

While an individual crystal structure reveals essential details of ligand—target interactions at atomic detail, it can provide only limited dynamic information. In silico simulations, on the other hand, suffer from the fact that it is time- and ensemble-averaged properties that may be verified by experiment, leaving the details in question. We show here that essential binding interactions of VX680 with Aurora involve flexibility and conformations that are not simply assignable to individual activation or complexation states of the kinase. The lessons are applicable to not only to VX680 analogues, such as VE465 now in preclinical trials, but to protein kinase inhibitor discovery programs in general.

AUTHOR INFORMATION

Corresponding Author

*Address: Institutt for kjemi, Universitetet i Tromsø, 9037 Tromsø, Norway. E-mail: Richard.Engh@uit.no.

ACKNOWLEDGMENT

We wish to thank Annica Hedberg and Prof. Dr. Ole Peter Rekvig for assistance with SPR measurements and the high performance computing centre of the University of Tromsø for computing time on the Stallo supercomputer.

ABBREVIATIONS USED

Abl, Abselson tyrosine kinase; AuA, Aurora A; BCR, breakpoint cluster region; FLT3, FMS-like tyrosine kinase-3; PDGFRA, alpha-type platelet-derived growth factor; SPR, surface plasmon resonance; TPX2, targeting protein for Xklp2; VDW, van der Waals contribution from molecular mechanics; ELE, electrostatic energy as calculated by the force field; GB, reaction field energy; GAS, total gas-phase energy; GBSUR, nonpolar contribution to the solvation free energy calculated by an empirical model; GBSOL, sum of nonpolar and polar contributions to solvation and final estimated binding free energy

REFERENCES

(1) Koshland, D. E. *Proc. Natl. Acad. Sci. U.S.A.* **1958**, *44*, 98–104.
(2) Engh, R. A.; Brandstetter, H.; Sucher, G.; Eichinger, A.; Baumann, U.; Bode, W.; Huber, R.; Poll, T.; Rudolph, R.; Vondersaal, W. *Structure* **1996**, *4*, 1353–1362.
(3) Rauh, D.; Klebe, G.; Stubbs, M. T. *J. Mol. Biol.* **2004**, *335*, 1325–1341.
(4) Carlson, H. A. *Curr. Pharm. Des.* **2002**, *8*, 1571–1578.
(5) Lundqvist, T. *Curr. Opin. Drug Discovery Dev.* **2005**, *8*, 513–519.
(6) Cavasotto, C. N.; Abagyan, R. A. *J. Mol. Biol.* **2004**, *337*, 209–225.
(7) May, A.; Zacharias, M. *J. Med. Chem.* **2008**, *51*, 3499–3506.
(8) Engh, R. A.; Bossemeyer, D. *Pharmacol. Ther.* **2002**, *93*, 99–111.
(9) Huse, M.; Kuriyan, J. *Cell* **2002**, *109*, 275–282.
(10) Eswaran, J.; Knapp, S. *Biochim. Biophys. Acta* **2010**, *1804*, 429–432.
(11) Cohen, P. *Nat. Rev. Drug Discovery* **2002**, *1*, 309–315.
(12) Johnson, L. N. *Q. Rev. Biophys.* **2009**, *42*, 1–40.
(13) Carvajal, R. D.; Tse, A.; Schwartz, G. K. *Clin. Cancer Res.* **2006**, *12*, 6869–6875.
(14) Fu, J.; Bian, M.; Jiang, Q.; Zhang, C. *Mol. Cancer Res.* **2007**, *5*, 1–10.
(15) Kitzen, J.; de Jonge, M.; Verweij, J. *Crit. Rev. Oncol. Hematol.* **2010**, *73*, 99–110.
(16) Carter, T. A.; Wodicka, L. M.; Shah, N. P.; Velasco, A. M.; Fabian, M. A.; Treiber, D. K.; Milanov, Z. V.; Atteridge, C. E.; Biggs, W. H.; Edeen, P. T.; Floyd, M.; Ford, J. M.; Grotzfeld, R. M.; Herrgard, S.; Insko, D. E.; Mehta, S. A.; Patel, H. K.; Pao, W.; Sawyers, C. L.; Varmus, H.; Zarrinkar, P. P.; Lockhart, D. J. *Proc. Natl. Acad. Sci. U.S.A.* **2005**, *102*, 11011–11016.
(17) Lin, Z.; Hsu, H.; Hsu, C.; Yeh, P.; Huang, C. F.; Huang, Y.; Chen, T.; Kuo, S.; Hsu, C.; Hu, F.; Jeng, Y.; Chung, Y.; Cheng, A. *J. Hepatol.* **2009**, *50*, 518–527.
(18) Cheetham, G. M.; Charlton, P. A.; Golec, J. M.; Pollard, J. R. *Cancer Lett.* **2007**, *251*, 323–329.
(19) Zhao, B.; Smallwood, A.; Yang, J.; Koretke, K.; Nurse, K.; Calamari, A.; Kirkpatrick, R. B.; Lai, Z. *Protein Sci.* **2008**, *17*, 1791–1797.
(20) Bossemeyer, D.; Engh, R. A.; Kinzel, V.; Ponstingl, H.; Huber, R. *EMBO J.* **1993**, *12*, 849–859.
(21) Bossemeyer, D. *Trends Biochem. Sci.* **1994**, *19*, 201–205.
(22) Grant, B. D.; Hemmer, W.; Tsigelny, I.; Adams, J. A.; Taylor, S. S. *Biochemistry* **1998**, *37*, 7708–7715.
(23) Neidle, S. *Cancer drug design and discovery*; Academic Press: New York, 2008.
(24) Yamaguchi, H.; Kasa, M.; Amano, M.; Kaibuchi, K.; Hakoshima, T. *Structure* **2006**, *14*, 589–600.
(25) Mohammadi, M.; McMahon, G.; Sun, L.; Tang, C.; Hirth, P.; Yeh, B. K.; Hubbard, S. R.; Schlessinger, J. *Science* **1997**, *276*, 955–960.
(26) Prade, L.; Engh, R. A.; Girod, A.; Kinzel, V.; Huber, R.; Bossemeyer, D. *Structure* **1997**, *5*, 1627–1637.
(27) Roumiantsev, S.; Shah, N. P.; Gorre, M. E.; Nicoll, J.; Brasher, B. B.; Sawyers, C. L.; Van Etten, R. A. *Proc. Natl. Acad. Sci. U.S.A.* **2002**, *99*, 10700–10705.
(28) Krishnamurty, R.; Maly, D. J. *ACS Chem. Biol.* **2010**, *5*, 121–138.
(29) Gorantia, S. P.; von Bubnoff, N.; Peschel, C.; Duyster, J. *Blood* **2008**, *112*, 3729.
(30) Cook, P. F. *Biochemistry* **1982**, *21*, 113–116.
(31) Bayliss, R.; Sardon, T.; Vernos, I.; Conti, E. *Mol. Cell* **2003**, *12*, 851–862.
(32) Case, D. A.; Darden, T. A.; Cheatham, T. E., III; Simmerling, C. L.; Wang, J.; Duke, R. E.; Luo, R.; Crowley, M.; Walker, R. C.; Zhang, W.; Merz, K. M.; Wang, B.; Hayik, S.; Roitberg, A.; Seabra, G.; Kolossváry, I.; Wong, K. F.; Paesani, F.; Vanicek, J.; Wu, X.; Brozell, S. R.; Steinbrecher, T.; Gohlke, H.; Yang, L.; Tan, C.; Mongan, J.; Hornak, V.; Cui, G.; Mathews, D. H.; Seetin, M. G.; Sagui, C.; Babin, V.; Kollman, P. A. *AMBER 10*; University of California: San Francisco, CA, 2008.
(33) Homeyer, N.; Essigke, T.; Meiselbach, H.; Ullmann, G. M.; Sticht, H. *J. Mol. Model.* **2007**, *13*, 431–444.
(34) Harrington, E. A.; Bebbington, D.; Moore, J.; Rasmussen, R. K.; Ajose-Adeogun, A. O.; Nakayama, T.; Graham, J. A.; Demur, C.; Hercend, T.; Diu-Hercend, A.; Su, M.; Golec, J. M. C.; Miller, K. M. *Nat. Med.* **2004**, *10*, 262–267.
(35) McGaughey, G. B.; Gagné, M.; Rappé, A. K. *J. Biol. Chem.* **1998**, *273*, 15458–15463.
(36) Grimme, S. *Angew. Chem., Int. Ed.* **2008**, *47*, 3430–3434.
(37) Fancelli, D.; Moll, J.; Varasi, M.; Bravo, R.; Artico, R.; Berta, D.; Bindi, S.; Cameron, A.; Candiani, I.; Cappella, P.; Carpinelli, P.; Croci, W.; Forte, B.; Giorgini, M. L.; Klapwijk, J.; Marsiglio, A.; Pesenti, E.;

628 Rocchetti, M.; Roletto, F.; Severino, D.; Soncini, C.; Storici, P.; Tonani,
629 R.; Zugnoni, P.; Vianello, P. *J. Med. Chem.* **2006**, *49*, 7247–7251.
630 (38) Bibby, R. A.; Tang, C.; Faisal, A.; Drosopoulos, K.; Lubbe, S.;
631 Houlston, R.; Bayliss, R.; Linardopoulos, S. *J. Biol. Chem.* **2009**, *284*,
632 33177.
633 (39) Aliagas-Martin, I.; Burdick, D.; Corson, L.; Dotson, J.;
634 Drummond, J.; Fields, C.; Huang, O. W.; Hunsaker, T.; Kleinheinz,
635 T.; Krueger, E.; Liang, J.; Moffat, J.; Phillips, G.; Pulk, R.; Rawson, T. E.;
636 Ultsch, M.; Walker, L.; Wiesmann, C.; Zhang, B.; Zhu, B.; Cochran, A. G.
637 *J. Med. Chem.* **2009**, *52*, 3300–3307.
638 (40) Rawson, T. E.; Rüth, M.; Blackwood, E.; Burdick, D.; Corson, L.;
639 Dotson, J.; Drummond, J.; Fields, C.; Georges, G. J.; Goller, B.; Halladay, J.;
640 Hunsaker, T.; Kleinheinz, T.; Krell, H.; Li, J.; Liang, J.; Limberg, A.;
641 McNutt, A.; Moffat, J.; Phillips, G.; Ran, Y.; Safina, B.; Ultsch, M.; Walker,
642 L.; Wiesmann, C.; Zhang, B.; Zhou, A.; Zhu, B.; Rüger, P.; Cochran, A. G. *J.*
643 *Med. Chem.* **2008**, *51*, 4465–4475.
644 (41) Cheetham, G. M. T.; Knegtel, R. M. A.; Coll, J. T.; Renwick,
645 S. B.; Swenson, L.; Weber, P.; Lippke, J. A.; Austen, D. A. *J. Biol. Chem.*
646 **2002**, *277*, 42419–42422.
647 (42) Cancilla, M. T.; He, M. M.; Viswanathan, N.; Simmons, R. L.;
648 Taylor, M.; Fung, A. D.; Cao, K.; Erlanson, D. A. *Bioorg. Med. Chem. Lett.*
649 **2008**, *18*, 3978–3981.
650 (43) Howard, S.; Berdini, V.; Boulstridge, J. A.; Carr, M. G.; Cross,
651 D. M.; Curry, J.; Devine, L. A.; Early, T. R.; Fazal, L.; Gill, A. L.;
652 Heathcote, M.; Maman, S.; Matthews, J. E.; McMenamin, R. L.; Navarro,
653 E. F.; O'Brien, M. A.; O'Reilly, M.; Rees, D. C.; Reule, M.; Tisi, D.;
654 Williams, G.; Vinković, M.; Wyatt, P. G. *J. Med. Chem.* **2009**, *52*,
655 379–388.
656 (44) Cee, V. J.; Cheng, A. C.; Romero, K.; Bellon, S.; Mohr, C.;
657 Whittington, D. A.; Bak, A.; Bready, J.; Caenepeel, S.; Coxon, A.; Deak,
658 H. L.; Fretland, J.; Gu, Y.; Hodous, B. L.; Huang, X.; Kim, J. L.; Lin, J.;
659 Long, A. M.; Nguyen, H.; Olivieri, P. R.; Patel, V. F.; Wang, L.; Zhou, Y.;
660 Hughes, P.; Geuns-Meyer, S. *Bioorg. Med. Chem. Lett.* **2009**, *19*,
661 424–427.
662 (45) Heron, N. M.; Anderson, M.; Blowers, D. P.; Breed, J.; Eden,
663 J. M.; Green, S.; Hill, G. B.; Johnson, T.; Jung, F. H.; McMiken, H. H. J.;
664 Mortlock, A. A.; Pannifer, A. D.; Pauptit, R. A.; Pink, J.; Roberts, N. J.;
665 Rowsell, S. *Bioorg. Med. Chem. Lett.* **2006**, *16*, 1320–1323.
666 (46) Coumar, M. S.; Leou, J.; Shukla, P.; Wu, J.; Dixit, A. K.; Lin, W.;
667 Chang, C.; Lien, T.; Tan, U.; Chen, C.; Hsu, J. T.; Chao, Y.; Wu, S.;
668 Hsieh, H. *J. Med. Chem.* **2009**, *52*, 1050–1062.
669 (47) Nowakowski, J.; Cronin, C. N.; McRee, D. E.; Knuth, M. W.;
670 Nelson, C. G.; Pavletich, N. P.; Rogers, J.; Sang, B.; Scheibe, D. N.;
671 Swanson, R. V.; Thompson, D. A. *Structure* **2002**, *10*, 1659–1667.
672 (48) Young, M. A.; Shah, N. P.; Chao, L. H.; Seeliger, M.; Milanov,
673 Z. V.; Biggs, W. H.; Treiber, D. K.; Patel, H. K.; Zarrinkar, P. P.;
674 Lockhart, D. J.; Sawyers, C. L.; Kuriyan, J. *Cancer Res.* **2006**, *66*, 1007–1014.
675 (49) Burley, S. K.; Petsko, G. A. *Science* **1985**, *229*, 23–28.
676 (50) Meyer, E. A.; Castellano, R. K.; Diederich, F. *Angew. Chem., Int.*
677 *Ed.* **2003**, *42*, 1210–1250.
678 (51) Gervasio, F. L.; Chelli, R.; Procacci, P.; Schettino, V. *Proteins:*
679 *Struct., Funct., Genet.* **2002**, *48*, 117–125.
680 (52) Eyal, E.; Gerzon, S.; Potapov, V.; Edelman, M.; Sobolev, V.
681 *J. Mol. Biol.* **2005**, *351*, 431–442.
682 (53) Cavallo, L.; Kleinjung, J.; Fraternali, F. *Nucleic Acids Res.* **2003**,
683 *31*, 3364–3366.
684 (54) Anderson, K.; Yang, J.; Koretke, K.; Nurse, K.; Calamari, A.;
685 Kirkpatrick, R. B.; Patrick, D.; Silva, D.; Tummino, P. J.; Copeland, R. A.;
686 Lai, Z. *Biochemistry* **2007**, *46*, 10287–10295.
687 (55) Bebbington, D.; Binch, H.; Charrier, J.; Everitt, S.; Fraysse, D.;
688 Golec, J.; Kay, D.; Knegtel, R.; Mak, C.; Mazzei, F.; Miller, A.;
689 Mortimore, M.; O'Donnell, M.; Patel, S.; Pierard, F.; Pinder, J.; Pollard,
690 J.; Ramaya, S.; Robinson, D.; Rutherford, A.; Studley, J.; Westcott, J.
691 *Bioorg. Med. Chem. Lett.* **2009**, *19*, 3586–3592.
692 (56) Lovell, S. C.; Davis, I. W.; Arendall, W. B., III.; de Bakker,
693 P. I. W.; Word, J. M.; Prisant, M. G.; Richardson, J. S.; Richardson, D. C.
694 *Proteins* **2003**, *50*, 437–450.